Failure Analysis of Rapid Prototyped Tooling in Sheet Metal Forming—Cylindrical Cup Drawing

Y. Park[1]

J. S. Colton
Professor, Fellow ASME

The George W. Woodruff School of Mechanical Engineering,
Georgia Institute of Technology,
Atlanta, GA 30332-0405

This paper presents a failure analysis of cylindrical cup drawing dies machined from a polymer composite rapid tooling material. Cup drawing is a complicated process, involving both bending and stretching. In this study, possible die failure modes are identified experimentally. Finite element analyses (FEA) are performed to obtain the stress–strain responses, which are used to determine the dominant failure mode. As cup drawing involves interactions among process parameters, the statistical design of experiments is employed to perform a parametric study. The resulting die failure mode estimation method is verified through experiments. [DOI: 10.1115/1.1828054]

1 Introduction

Drawing is a process of forming a flat, pre-cut, metal blank into a hollow shape, either cylindrical or box-shaped, by pressing it into a die cavity without excessive wrinkling, thinning, or fracturing. Typical parts produced by drawing include beverage cans, containers of all shapes and sizes, and automobile and aircraft panels. Due to the versatility of the geometries and sizes of the parts that can be achieved, aluminum trihydrate (ATH)-filled polyurethane tooling board has been used widely in sheet metal drawing industries, and Ren Shape™ 5166 is such a material. ATH exists in a powder form at room temperature and has a typical particle size of 3–4 μm. The spherical ATH is randomly dispersed in the matrix to impart material isotropy and adhesion. More importantly, ATH serves to increase the overall compressive strength and to improve tribological characteristics. A number of automobile panel and aircraft part industries reported that the use of ATH-filled polyurethane contributed to reducing the die fabrication time from months to days (or even to hours), thus slashing the overall production cost [1,2]. Other commonly used rapid tooling materials, such as aluminum-filled epoxy, photosensitive resin, and Kirksite, tend to exhibit mechanical behavior similar to Ren Shape™ 5166, especially high compressive strength (as compared to tensile strength) and brittle nature [3,4].

However, due to their lack of strength as compared to conventional die materials, the premature failure of polymer composite dies is an issue. For example, Park [5] compared the stress states in V-bending dies made from Ren Shape™ 5166 and conventional die steel. He found that under identical forming conditions, higher stress is concentrated in the steel die due to its higher stiffness and therefore less capability to absorb and distribute strain energy. However, the stress level in the Ren Shape™ 5166 die is significantly higher relative to its tensile strength, which makes it more prone to premature failure. These dies have been designed based on the guidelines established for metal dies, which often leads to geometry and dimensions that are not suitable for polymer composite dies. Consequently, a significant portion of time in the design stage must be allotted to the die tryout process, which demerits the advantages of advanced die materials and runs contrary to the whole concept of ''rapid'' tooling. Therefore, there has been a strong demand for a method to estimate tool life and to take measures necessary to increase tool life during the tool design phase.

Unlike bulk metal forming, in sheet metal forming bending and stretching in plane stress conditions are the dominant mechanisms, and elongation, anisotropy, residual stress, and springback are considered to be significant factors. As the two types of metal forming processes are governed by fundamentally different mechanisms, the forming conditions to which the dies are subjected must be different. It is true that many studies have dealt with the sheet metal itself in terms of formability and defects. However, not much attention has been paid to the failure and life prediction of sheet metal forming dies.

Accordingly, there have been rather a limited number of studies in tool failure in sheet metal forming. Jensen et al. [6,7] developed a semi-empirical wear model to obtain the distribution of tool wear on the die profile in deep drawing. The key idea was that wear was treated as a location- and time-dependent problem. The model states that the volume of wear depends on the tangential velocity of the blank and the normal pressure on the draw die profile. Using a wear model and a conventional optimization technique in conjunction with the finite element method, they performed an optimization of an elliptical draw die profile. The study revealed that the strain-hardening coefficient and the thickness of the sheet metal and draw ratio greatly influence wear.

The progressive wear and other surface alteration processes that take place on deep drawing dies were analyzed in detail by Christiansen and de Chiffre [8]. The authors developed a theory relating various surface alteration processes, such as ploughing and adhesion, and surface roughness parameters. They found that the maximum wear takes place at angular positions of 20 deg and 70 deg along the die corner radius, with the minimum at 45 deg. Furthermore, they observed that progressive wear is initiated by plowing after only a few drawing operations and this mechanism dominates until the die wears out.

Siegert and Haller [9] investigated various specialized tooling materials for prototype draw dies in automotive applications. They compared gray cast iron, bismuth/tin alloys, zinc alloys, and polymers, namely, pre-cast epoxies, polyurethanes, and polyamides. They conducted a wide range of material tests, including tension, compression, strip drawing friction, and wear. Based on the measurements of the depth of die wear and the effective strains in the part (in relation to part quality), the advantages and disadvantages of each material were discussed.

This paper proposes a computer-aided method to determine the failure mode of a cylindrical cup drawing die fabricated from Ren

[1]Currently at the Department of Industrial and Manufacturing Engineering, FAMU-FSU College of Engineering, Tallahassee, FL.

Contributed by the Manufacturing Engineering Division for publication in the JOURNAL OF MANUFACTURING SCIENCE AND ENGINEERING. Manuscript received August 11, 2003; revised February 11, 2004. Associate Editor: J. Cao.

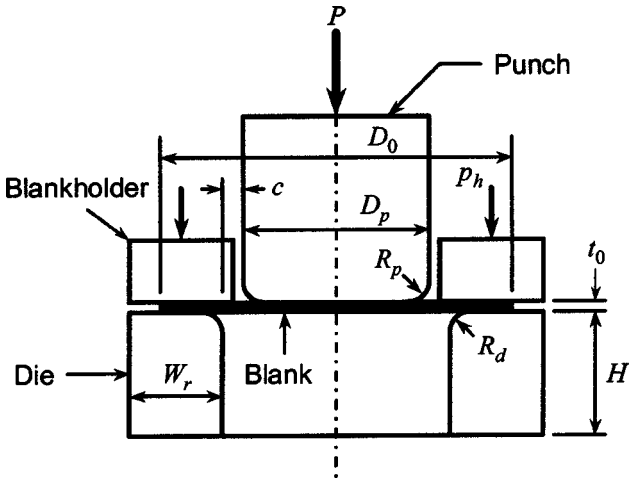

Fig. 1 Schematic of deep drawing

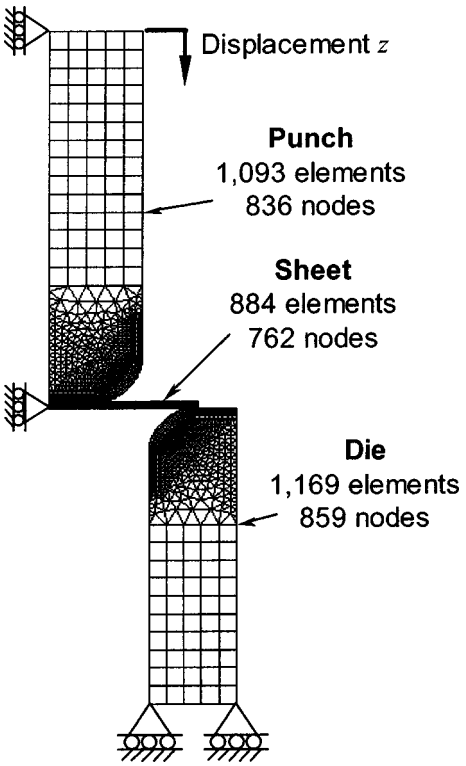

Fig. 2 FE model of cylindrical cup drawing

Shape™ 5166, a commercial ATH-filled polyurethane board stock developed for rapid tooling applications. Finite element analyses (FEA) were conducted, in conjunction with cup drawing experiments, to identify the stress states under which each failure mode dominates. A parametric study was performed using design of experiments to determine the dominant process parameters as well as multi-factor interactions. The resulting failure prediction method was verified through experiments. Finally, general tool design guidelines are proposed, which can be used in the preliminary die design stage.

2 Simulation of Cylindrical Cup Drawing

2.1 Mechanics of Cup Drawing. A schematic illustration of the cylindrical drawing process is shown in Fig. 1, consisting of punch, push-through die, blank, and blankholder. The basic parameters also are labeled, which include draw ratio DR (the ratio of the undeformed blank diameter D_0 to the diameter of the punch D_p), clearance between punch and die c, punch and die corner radii R_p and R_d, mechanical properties of sheet metal, sheet thickness t_0, blankholder pressure p_h, friction and lubrication at punch-die–workpiece interface, and punch speed v_p.

It is important to consider the metal's plastic flow that takes place during a drawing operation to assess drawability and to investigate the stresses in the punch and the die induced by the movement and the deformation of the workpiece. During the first stage, the blank is bent or wrapped around the punch nose, which usually occurs after a small stroke. Simultaneously and subsequently, the outer portion (or flange) of the blank moves radially towards the center. The various volume elements of the blank decreases accordingly in the circumferential direction until they reach the die bore. They bend to conform to the die corner radius and then unbend when they become tangent to the cup wall. A blankholder prevents the blank from flowing freely into the die cavity and thus may prevent wrinkling in the flange area.

The punch force is transmitted from the bottom of the cup to its wall, which is subjected to axial tensile stresses. The tensile stresses generate reactive stresses which (1) circumferentially compress and radially stretch the material in the flange, (2) bend and unbend the material flowing from the flange into the cup wall, and (3) overcome the frictional resistance under the blankholder and the inside wall of the die. Due to the local changes in the volume and resistance of the metal being formed, the punch force usually increases first, then passes through a maximum, and finally decreases gradually to zero [10].

2.2 Pre-Processing. Cylindrical cup drawing simulation was performed using ABAQUS/CAE. The problem was analyzed assuming that inertial effects were insignificant compared to stiffness effects. Figure 2 provides a detailed description of the ''base'' model. The model consisted of three parts: punch, die, and workpiece. As the process was axisymmetric, axisymmetric solid elements were used to model the parts. The consequence of using axisymmetric elements instead of the more general three-dimensional solid elements is that an axisymmetric simulation cannot predict wrinkling in the circumferential direction if there are significant circumferential compressive stresses. However, as this research was more concerned with the failure of dies in the absence of wrinkling, which may introduce an additional source of failure via high, localized contact pressure, a blankholder was excluded from the model (and also from the experiments discussed in the following sections) and axisymmetric elements were deemed appropriate.

The elastic properties of Ren Shape™ 5166 (i.e., Young's modulus of 7.2 GPa and Poisson's ratio of 0.34 [5]) were assigned to the punch and the die, and the sheet metal material was assumed to be aluminum 1100-O. Based on the metal-polymer friction coefficient determined by Park [5], a friction coefficient of 0.2 was assumed. The punch and die geometries were determined based on die design handbooks [11–13]. These guidelines provided the upper and lower limits for most design parameters in deep drawing. The design ranges, most of which depend on the blank thickness, are listed in Column A of Table 1 assuming a blank thickness of 1 mm. As for the actual values used in the FE model, intermediate values were selected if the upper and lower limits exist, and values slightly lower than the upper limit if only the upper limits were available. Among the design parameters, the strain factor E_c is the measure of thickening in the blank rim (due to compressive circumferential stresses) before it is drawn into the die cavity. The run-off W_r is the ''thickness'' of the die dictated by the inner and outer diameters (Fig. 1).

Figure 2 shows the mesh design used for the ''base'' model. The punch and the die were partitioned to impart different mesh schemes in different regions. One region, which was likely to be under the most critical state of stress, consisted of partitions that

Table 1 Process parameters for the "base" cup drawing model and the model for experimental FEA validation Al: aluminum, SS: stainless steel

Process Parameter	Symbol	Definition and Design Rule	A	B
Sheet material	N/A	N/A	1100-O Al	304 stainless steel
Sheet thickness	t_0	N/A	1 mm	1.22 mm
Blank diameter	D_0	N/A	50.8 mm	50.8 mm
Punch diameter	D_p	N/A	31.8 mm	28.6 mm
Draw ratio	DR	$\frac{D_0}{D_p}$ 1.8 max for Al, 2.0 max for SS	1.8	1.8
Reduction in diameter	RD	$100\left(1-\frac{D_p}{D_0}\right)$ 45% max for Al, 50% max for SS	44	44
Strain factor	E_c	$\frac{D_0/D_p+1}{2}$ 1.4 max for Al, 1.5 max for SS	1.4	1.4
Punch–die clearance	c	(1.08–1.10) t_0 for Al (t_0=0.4–1.27 mm) (1.75–2.25) t_0 for SS	1.09 mm	2.14 mm
Punch corner radius	R_p	(6–10) t_0	8 mm	6.4 mm
Die corner radius	R_d	(6–10) t_0	8 mm	6.4 mm
Run-off	W_r	N/A	15 mm	13 mm
Die height	H_d	N/A	50.8 mm	50.8 mm
Punch travel distance	d_p	N/A	30 mm	30 mm
Punch speed	v_p	N/A	120 mm/min	120 mm/min
Friction coefficient	μ	N/A	0.2	0.2
Miscellaneous	N/A	N/A	Axisymmetric	Axisymmetric

made up a thin layer near the corner radii. The layer was 2 mm thick, and the mesh was most dense in this region. The "base" model contained 1093, 1169, and 884 elements and 836, 856, and 762 nodes in the punch, die, and sheet, respectively. There were five elements in the sheet thickness direction. The nodes along the centerline of symmetry and those on the bottom surface of the die were constrained in the horizontal and vertical directions, respectively.

2.3 FE Model Validation: Computational. The FE model was validated using various computational methods, including stress analysis and drawing force (or punch force) considerations. In drawing, it is not easy to identify a priori where the most severe stress state (in the die) occurs. The stresses in the die and the sheet metal, which move relative to each other, must be tracked throughout the process to define the location and the magnitude of the maximum (or critical) stress.

An iterative mesh refinement technique was employed to determine the optimal mesh density in the FE model. The minimum mesh size within the 2-mm-thick layer of the corner radius regions was varied between 0.1 and 0.6 mm by increments of 0.1 mm. First, the punch force was plotted versus time for each mesh size by summing the reaction forces at the nodes on the bottom surface of the die. All six mesh sizes yielded essentially the same force curve, which indicates that mesh size has no substantial influence on the force transmitted from punch top to die bottom. Second, the maximum magnitudes of the normal (CPRESS) and shear (CSHEAR) components of the contact stress on the bottom surface of the sheet metal were plotted at the end of the downward movement of the punch. Both stresses leveled off when the minimum mesh size has been reduced to below 0.3 mm. In conclusion, 0.3 mm represents the optimal mesh size in terms of both computational efficiency and solution accuracy.

Another method to validate the FEA results was to check if they made physical sense. The physical interpretation begins with the investigation of the stress fields that result from the process simulation. Figure 3(*a*) shows the punch–workpiece–die configuration when the highest maximum principal stress in the die occurs, and Fig. 3(*b*) shows the maximum principal stress distribution in the isolated die. Only the die was considered because the magnitudes of both the maximum and minimum principal stresses in the punch were significantly lower than those in the die, which suggests that the die is likely to fail sooner than the punch. The two figures suggest that the greatest maximum principal stress occurs at the lower end of the die corner radius when the sheet has just drawn into the die cavity (at the simulation time of 12.03 sec). This is due to the fact that the lip that forms around the edge of the blank plows the die surface as the blank completes its entry into the straight section of the die cavity. The lowest minimum principal stress takes place slightly above the die corner end at 11.03 sec, and its magnitude is greater than that of the highest maximum principal stress by almost a factor of five (Fig. 3(*c*)). It is important to point out that the maximum principal direction coincides with the circumferential (or "hoop") direction.

3 Failure in Drawing Dies

3.1 Fracture. The failure of a cylindrical cup drawing die can be analyzed in a manner similar to an internally loaded ring or thick-walled cylinder. Kocanda and Raddad [14] performed physical and analytical modeling of the deformation of ring-shaped steel dies loaded by inner pressure. They employed the ring expansion test to find the relationship between the fracture load for the ring, the maximum stress at fracture, and the material properties of the die material. The authors obtained the maximum equivalent stress at die fracture from FEA and related it to the uniaxial yield strength of the die material. They verified that the stresses predicted by the FEA agreed with the well-known Lamé's analytical solution for thick-walled cylinders.

A similar method can be used for Ren Shape™ 5166. A typical drawing force curve to the fracture of a ring-shaped Ren Shape™ 5166 die (obtained experimentally) is shown in Fig. 4. As the drawing process progresses, the force increases, reaches a peak, and begins to drop until it reaches the fracture point. Figure 5 shows the punch–sheet–die configurations at both the maximum drawing force and at the die fracture (obtained from the FE model described in Section 2.2). The peak in the force curve (in Fig. 4) corresponds to the instant at which the edge of the blank has cleared 1/4 of the die corner radius as shown in Fig. 5(*a*). One important observation is that the fracture point does not coincide with the point of maximum load (it actually occurs past this point), and this phenomenon necessitates the investigation of the stresses. Because a low-ductility die material is used, the maximum principal stress, instead of the equivalent stress, is considered. Figure 6(*a*) plots the stresses as a function of the distance from the die corner exit along the corner radius for cup drawing

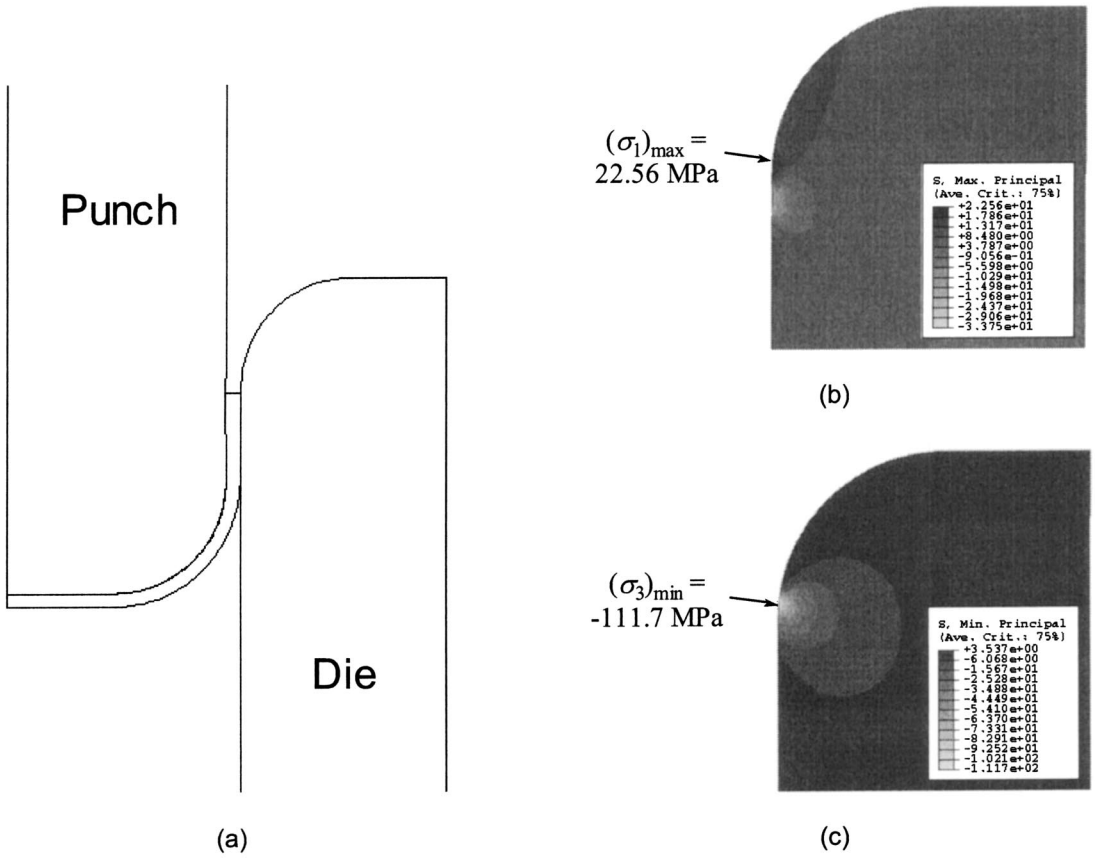

Fig. 3 Stress distributions in the cup drawing die: (*a*) configuration; (*b*) maximum principal stress distribution (12.03 sec); (*c*) minimum principal stress distribution (11.03 sec)

with Ren Shape™ 5166, using the FE model described in Section 2.2. The greatest maximum principal stress occurs at fracture (at 8.712 sec), 2.5 mm from the die corner exit, rather than at the point of maximum force (at 7.375 sec). There were five time steps between these two instants, which warrants that the peak of the curves were being captured accurately. As shown in Fig. 6(*a*), the magnitude of the highest maximum principal stress satisfies the approximation in Eq. (1) (determined empirically by the authors)

$$(\sigma_1)_{\max} \approx \sigma_u = 1.6\sigma_{uts} \tag{1}$$

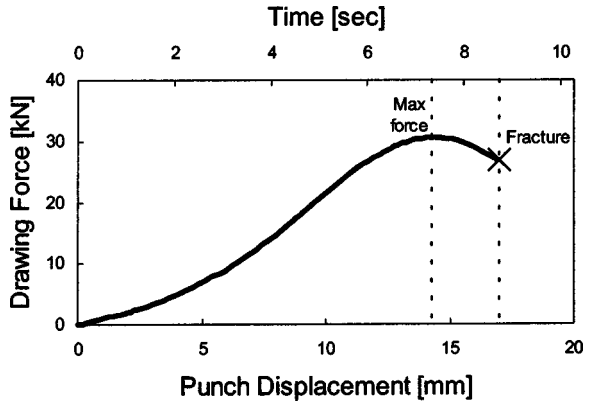

Fig. 4 Force curve for a typical drawing process up to die fracture

where σ_u is the flexural strength and σ_{uts} is the ultimate tensile strength. The curves in Fig. 6(*a*) indicate the complex nature of the stress states in the dies, which depend on the time of the process and the location in the die.

3.2 Plastic Deformation. If the die sustains the punch load in the first several drawing trials, it is not likely to fail by catastrophic fracture in subsequent drawing cycles. Therefore, plastic deformation and wear become issues. Although Ren Shape™ 5166 can be classified as a brittle solid, the standard tension and compression tests performed by Park [5] revealed that plasticity can be influential when the material is in compression. When the magnitude of the compressive stress exceeds the compressive yield strength, plastic deformation occurs within the material.

Ideally, as the blank is drawn into the bore of the die, the stress distribution around the perimeter of the die entrance is uniform. However, in practice, the stresses may not be uniform due to a number of reasons, such as punch–die misalignment, anisotropy of the sheet metal and the die material, nonuniform lubrication or tribological conditions, and geometric irregularity due to die fabrication errors. A nonuniform stress distribution can lead to localized plastic deformation in the die. The final geometry of the drawn part is particularly sensitive to the die defect because they lead directly to wrinkling (in the case where no blankholder is used). Once the uniformity of the stress distribution is disturbed, the metal flow becomes ''unstable'' and the degree of wrinkling increases with each drawing cycle, as the size of the defect grows.

Part defects due to localized plastic deformation in the die are not process-inherent phenomena, as they can be prevented by proper punch–die alignment, material selection and handling, and

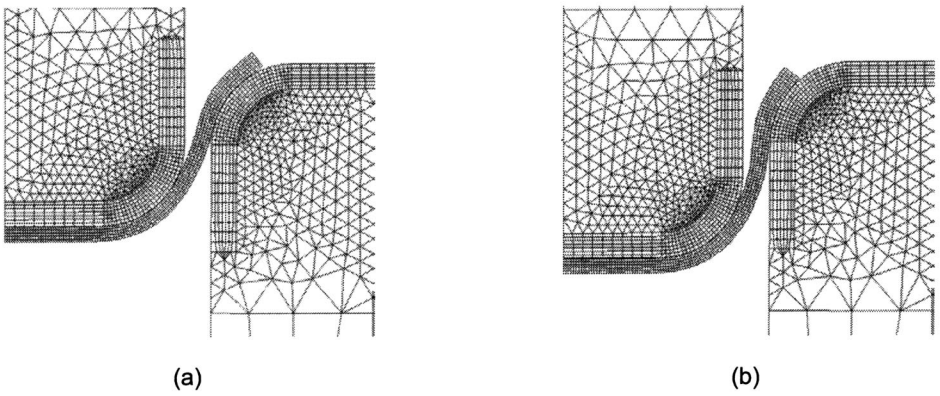

Fig. 5 Punch–sheet–die configurations: (*a*) at maximum drawing force; (*b*) at fracture

lubrication. However, care must be taken to select design and process parameters so as not to exceed the compressive yield strength of the die.

3.3 Wear. While fracture and plastic deformation can be considered design flaw-induced failures, wear is a more "natural" mode of die failure, which often determines the service life. Wear occurs when two solid surfaces in contact slide relative to each other. Wear processes are classified into four main categories: abrasion, adhesion, surface fatigue, and tribochemical wear [15]. Adhesive wear occurs when mating surfaces slide against each other, and fragments of one surface pull off and adhere to the other. Abrasive wear occurs when harder surfaces scrape or abrade away the mating surface, and is often characterized by grooves, gouges, or pits. Fatigue wear occurs when the pressure or velocity exceeds the capabilities of the mating surfaces, resulting in a melted, deformed, embrittled, or fractured part. In principle, ideal elastic solids with no surface defects should show no fatigue wear [16]. But with real materials, surface or subsurface microcracks are formed and eventually grow into large cracks. Tribochemical wear is associated with chemical reactions with the environment.

The primary wear mechanism for polymer–metal contact is adhesive wear, often accompanied by abrasive wear. Adhesive wear is characterized by the formation of a coherent transferred layer on the metal counterpart [15]. The adhesive forces between the polymer and the mating part are sufficient to inhibit sliding at the original interface. The adhesive junctions, which form at the real areas of contact, rupture within the polymer itself and a layer of polymer is deposited on the counterface. Adhesive wear can be quantified based on the probability that a junction between two sliding surfaces would lead to the formation of a wear particle using Archard's expression (Eq. (2))

$$V = k\frac{lw}{h} \tag{2}$$

where V is the volume of material removed by wear from the surface, k is the wear coefficient (dimensionless), l is the sliding length, w is the normal load, and h is the local hardness of the softer body (in the unit of pressure). For a given drawing process at a given instant, k, l, and h may be considered constant, and therefore the wear volume is governed by the normal load. It is rather difficult to detect and predict wear, and is beyond the scope of this research. However, the normal stresses along the die corner radius, which bear a direct relation to the normal load, is used as a measure of the severity of the sliding conditions in a later section.

Abrasive wear occurs in drawing dies when the blank has poor surface roughness. Poor surface roughness originates from several different sources, such as hard, protruding particles, which are often residues from high-energy blanking operations (for example, plasma-arc cutting for nonferrous alloys), scratches, and oxidized layers. Abrasive wear can be controlled effectively if these surface impurities and burrs on the blank edges are eliminated.

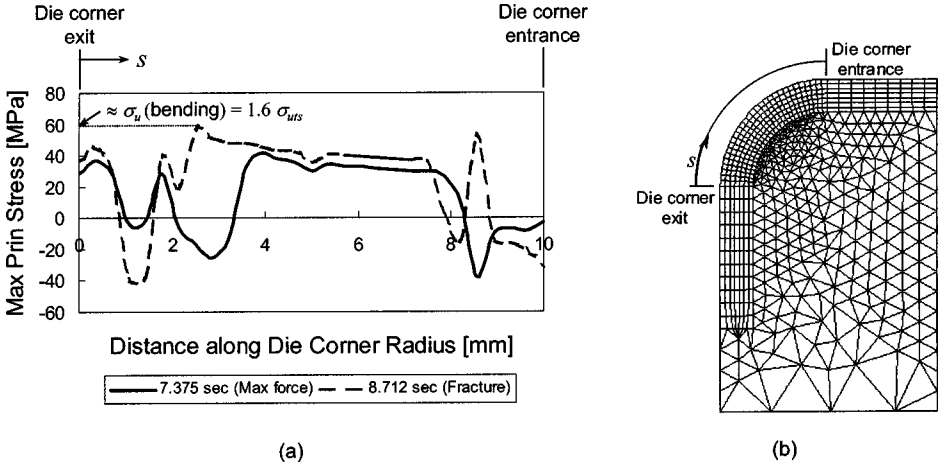

Fig. 6 Stresses along the die corner radius: (*a*) maximum principal stress curves; (*b*) definition of "distance"

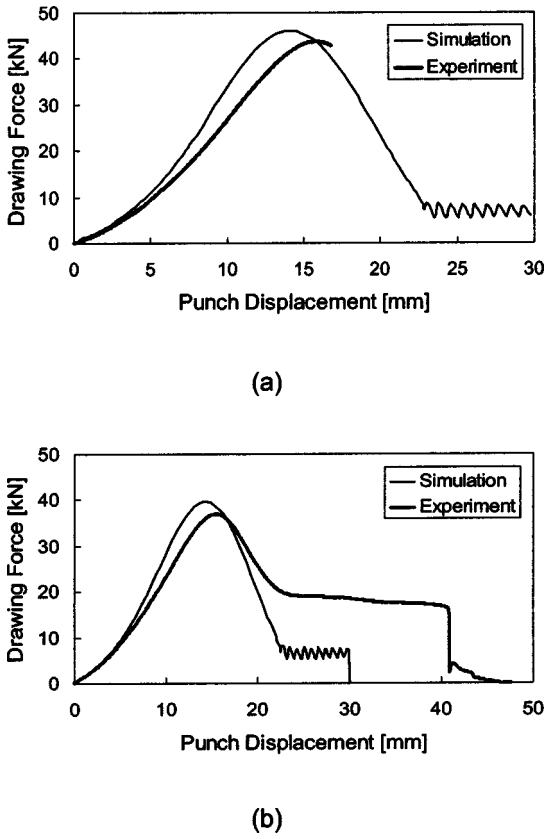

Fig. 7 A comparison of drawing forces: (*a*) Case 1; (*b*) Case 2

4 Experimental Methods

4.1 Experimental Setup. An MTS Model 851.62 axial-torsional material test system, equipped with a 250 kN load cell, was used to perform the cylindrical cup drawing tests.

4.2 FE Model Validation: Experimental. In order to validate the FE model experimentally, cup drawing experiments were performed and the drawing force curves were compared with those obtained from simulation. The sheet material used was 304 stainless steel. Its constitutive behavior was modeled as power law hardening, $\tilde{\sigma}=1275\tilde{\varepsilon}^{0.45}$ (MPa) [11]. The sheet thickness was 1.22 mm (0.048 in.). The punch and die corner radii were 6.4 mm (0.25 in.). The relevant process parameters are summarized in Column B of Table 1.

The FEA and corresponding cup drawing experiments were performed using the parameters listed in Column B of Table 1. Two cases were considered, in both of which the time histories of the drawing force were compared. In the first case, the values exactly shown in Column B of Table 1 were used, and the resulting drawing forces are plotted in Fig. 7(*a*). The force curves exhibit similar trends as well as maximum values, which are indicative of the accuracy of the FE model developed. Note the termination of the experimental force curve as soon as it passes its peak, which coincides with the fracture of the die. An important thing to keep in mind is that the point of maximum drawing force does not necessarily coincide with the most severe state of stress, which leads to die fracture, as discussed in Section 3.1. Rather, die rupture is more closely associated with the instant and location of the maximum principal stress. The simulated force curve exhibits no sign of fracture because the die was modeled as an elastic, deformable body with no plasticity and fracture characteristics.

In the second case, a set of ''relaxed'' parameters was applied. All of the parameters in Column B of Table 1 were used except for the punch–die clearance was changed to $2.25t_0$ (or 2.75 mm) and the run-off to 15 mm. The two modifications were made to prevent catastrophic failure of the die. The resulting force curves are illustrated in Fig. 7(*b*). The curves show discrepancies after the sheet metal has cleared the die corner radius, which corresponds to the punch displacement of around 22 mm. This is most probably due to the difference between simulated and actual friction that occurs between the inner die surface and the edge of the sheet metal.

4.3 Design of Experiments. The statistical design of experiments method was employed to develop the design matrix to investigate the factor effects. Many of the die design rules in Table 1 are expressed in the form of a range, which suggests that a two-level factorial design is appropriate [17]. A two-level factorial design is especially useful when the number of factors is relatively large and the limits of the range of the factor are available. Among the parameters involved in cup drawing, seven geometric and material parameters were identified as the factors that might affect the stress state in the die, as listed in Table 2. The upper and lower limits of each factor were determined based on the rules provided by die design handbooks [11–13]. A uniform (undeformed) blank diameter (D_0) of 50.8 mm was used, and the draw ratio was controlled by varying the punch diameter (D_p).

Table 2 indicates that the factors are nested; that is, several factors (namely, R_p, R_d, and c) depend on another factor (t_0). In order to simplify the problem, several modifications were made in the process of level selection, as not all design rules could be accommodated. First, the same range was used for the punch and die corner radii, regardless of the sheet thickness. If the design guidelines were followed strictly, the blank thickness of 1.22 mm would yield the corner radius range of 7.32–12.2 mm. However, this range would cause the flat contact area between the blank and the die (that is, the flat area of the die on which the blank lies before deformation) to become negative, meaning that the undeformed blank diameter would be placed ''on'' the die corner, instead of on the flat surface. The largest allowable die corner radius (in the case of minimum draw ratio and maximum punch–die clearance) was calculated to be 6.11 mm. Therefore, the range of 3–6 mm was chosen, which satisfies the geometric compatibility and also is wide enough to demonstrate the effects of the radii.

Table 2 Upper and lower factor levels for process parameters

No	Factor	Symbol	Design rule	Low limit	High limit
1	Draw ratio	DR	1.8 max for Al 2.0 max for SS	1.45	1.78
2	Sheet thickness	t_0	N/A	0.4 mm	1.22 mm
3	Punch corner radius	R_p	(6–10) t_0	3 mm	6 mm
4	Die corner radius	R_d	(6–10) t_0	3 mm	6 mm
5	Sheet strength $(\sigma_Y+\sigma_{uts})$	N/A	N/A	1100-O Al (125 MPa)	304 SS (720 MPa)
6	Punch–die clearance	c	Al : (1.08–1.10) t_0 SS : (1.75–2.25) t_0	0.44 mm 1.34 mm	0.60 mm 1.83 mm
7	Run-off	W_r	N/A	10 mm	20 mm

Table 3 Design matrix for the parametric study of cylindrical cup drawing

	Factor							Response (MPa)	
	X_1	X_2	X_3	X_4	X_5	X_6	X_7	Y_1	Y_2
Treatment	DR	t_0	R_p	R_d	Strength	c	W_r	$(\sigma_1)_{\max}$	$(T_n)_{\max}$
1	−1	−1	−1	−1	−1	−1	−1	16.99	31.89
2	1	−1	−1	−1	1	−1	1	61.32	185.33
3	−1	1	−1	−1	1	1	−1	121.13	327.24
4	1	1	−1	−1	−1	1	1	20.22	67.01
5	−1	−1	1	−1	1	1	1	29.63	91.64
6	1	−1	1	−1	−1	1	−1	7.21	16.59
7	−1	1	1	−1	−1	−1	1	24.09	80.49
8	1	1	1	−1	1	−1	−1	171.77	584.39
9	−1	−1	−1	1	−1	1	1	3.40	9.88
10	1	−1	−1	1	1	1	−1	39.74	93.10
11	−1	1	−1	1	1	−1	1	160.02	428.70
12	1	1	−1	1	−1	−1	−1	22.28	142.49
13	−1	−1	1	1	1	−1	−1	34.46	105.83
14	1	−1	1	1	−1	−1	1	28.94	126.10
15	−1	1	1	1	−1	1	−1	13.24	37.96
16	1	1	1	1	1	1	1	183.61	478.60
P-values for $\sqrt{(\sigma_1)_{\max}}$	0.309	0.007	0.844	0.965	0.000	0.258	0.572		
P-values for $\sqrt{(T_n)_{\max}}$	0.092	0.000	0.655	0.824	0.000	0.057	0.548		

Another modification was that an identical rule was applied to the punch–die clearance for both types of material. Instead of applying separate rules for aluminum and stainless steel, which would yield eight different factor levels (as the clearance is a function of blank thickness as well), the range of (1.1–1.5) t_0 was used for both materials. This range was wide enough to capture the effect of the parameter.

A two-level, full factorial design would yield $2^7=128$ treatments, which is a prohibitive number to perform with FEA. Modifying the FE models tends to be extremely tedious, and the simulation run time would be unreasonably long. (A typical simulation would take about 40 minutes using Silicon Graphics Octane equipped with a single 600 MHz CPU.) In a fractional factorial design, a subset of the treatments is selected in such a way that most of the degrees of freedom for the study of factor effects are devoted to main effects and low-order interactions, at a cost of only some loss of information about higher-order interactions. In this study, a 2^{7-3}_{IV} fractional (one-eighth) factorial design was used, where 7 denotes the total number of factors, 3 the fraction (that is, $1/2^3=1/8$), and IV the design resolution. Table 3 shows a summary of the standard design matrix of the one-eighth fraction design for the two level, seven-factor experiment generated by the MINITAB Fractional Factorial procedure. The values −1 and 1 denote the low and high levels, respectively, for each factor. The response vectors also are shown in the last two columns of the table. Two damage parameters—the greatest maximum principal stress $(\sigma_1)_{\max}$ and the maximum normal component of the traction vector $(T_n)_{\max}$, both in MPa—that are relevant to fracture, plastic deformation, and wear in a drawing die are considered as the responses. As for $(T_n)_{\max}$, the absolute values were employed to facilitate the computation.

Two responses, $(\sigma_1)_{\max}$ and $(T_n)_{\max}$, were considered separately. In order to satisfy the constancy of error variance and normal probability requirements, which are necessary for the validity of the simple linear regression model and the subsequent analyses of variance (ANOVA), the square root of each response was taken. The regression results for the model based on main effects and $\sqrt{(\sigma_1)_{\max}}$, including the P-values, indicated that the main effects for sheet thickness t_0 and sheet strength are statistically significant (based on the cut-off value of 0.05). Draw ratio DR and punch–die clearance c also have significant influences on $\sqrt{(\sigma_1)_{\max}}$ to some degree, although their P-values were well above the cut-off value. As for $\sqrt{(T_n)_{\max}}$, the influences of sheet thickness and strength were more pronounced than in the case of $\sqrt{(\sigma_1)_{\max}}$. In addition, draw ratio and punch–die clearance had a much greater influence on $\sqrt{(T_n)_{\max}}$.

5 Results and Discussions

5.1 Parametric Study. The output for an initial fractional factorial design (i.e., the magnitude of the factor effect coefficients) involving the transformed responses, $\sqrt{(\sigma_1)_{\max}}$ and $\sqrt{(T_n)_{\max}}$, indicated that the active effects are main effects for sheet thickness and strength, and the two-factor interaction between draw ratio and punch corner radius (Table 4). Draw ratio

Table 4 MINITAB fractional factorial output for interactions

	Response $\sqrt{(\sigma_1)_{\max}}$		Response $\sqrt{(T_n)_{\max}}$	
Interaction	Estimated effect	Estimated coefficient	Estimated effect	Estimated coefficient
$DR-t_0$	−0.156	−0.078	0.292	0.146
$DR-R_p$	2.641	1.321	3.820	1.910
$DR-R_d$	0.414	0.207	0.829	0.414
DR–Strength	0.382	0.191	−0.105	−0.053
$DR-c$	0.202	0.101	−1.066	−0.533
$DR-W_r$	0.529	0.265	0.358	0.179
t_0-R_d	0.216	0.108	−0.018	−0.009
$DR-t_0-R_d$	−0.341	−0.170	−0.417	−0.208

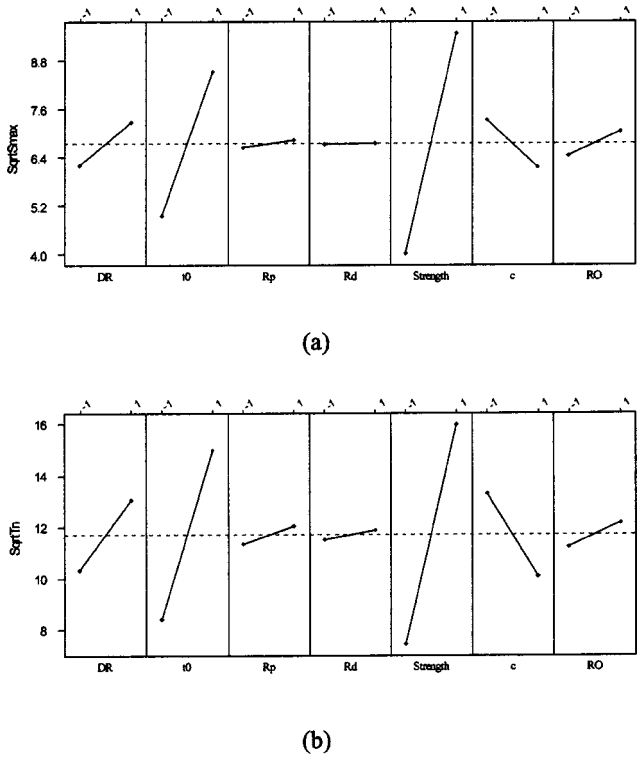

Fig. 8 Main effects plot for (*a*) $\sqrt{(\sigma_1)_{max}}$; (*b*) $\sqrt{(T_n)_{max}}$

and punch-die clearance also had moderate effects. The main effects on $\sqrt{(\sigma_1)_{max}}$ and $\sqrt{(T_n)_{max}}$ are graphically represented in Fig. 8.

Out of 21 possible two-factor combinations, three interactions were significant—namely, $DR-R_p$, t_0-Strength, and R_d-W_r interactions. The interaction plots for the three combinations are shown in Fig. 9. At high draw ratio, the mean stress increases as the punch corner radius increases. Conversely, at a low draw ratio, the mean stress decreases as the punch corner radius increases. Increasing the sheet strength tends to increase the stress at all levels of draw ratio, sheet thickness, and punch and die corner radii. However, as for sheet thickness, this trend is more prominent at the high level than the low level. Therefore, from a design standpoint, using a high-strength, large-thickness sheet metal would be most detrimental to die life. The R_d-W_r interaction exhibits similar trends as the $DR-R_p$ interaction. Increasing run-off at a high level of the die corner radius increases stress and vice versa.

5.2 Experimental Results.

Fracture. Dies with various dimensions were fabricated to determine the effects of punch–die clearance and run-off on die fracture. The significances of punch–die clearance and runoff were discovered experimentally. The initial challenge was to determine the conditions under which the die fails by catastrophic fracture due to overload before other failure mechanisms predominate. The following two sets, each consisting of three experiments, as specified in Table 5, were performed to investigate the influences of punch–die clearance and run-off. The authors were more concerned with determining the threshold punch force at which the die breaks, verifying the failure criteria, and validating the simulation results, rather than specifically verifying the parametric study results.

In order to induce fracture, relatively severe conditions were applied, that is, high-strength sheet material, large sheet thickness, and large draw ratio. (Another reason for using a large-thickness sheet metal was to minimize wrinkling.) As shown in Table 1, the

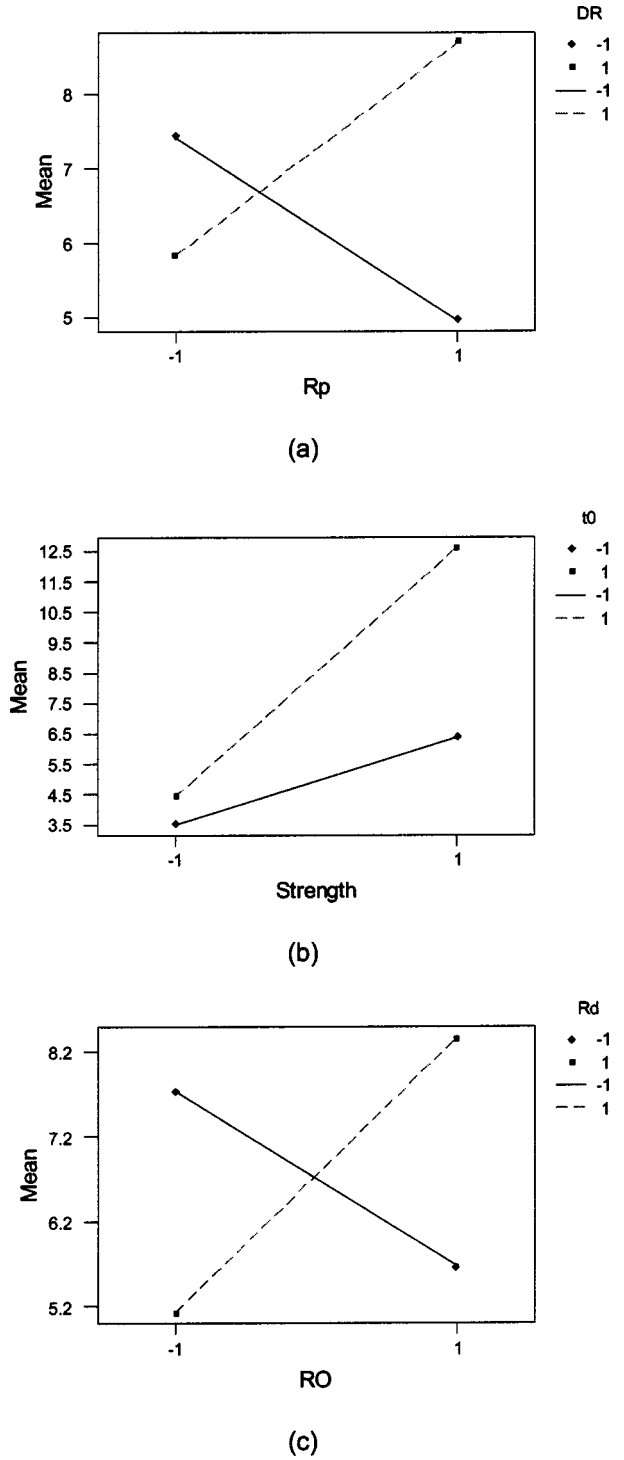

Fig. 9 Influential two-factor interactions for $\sqrt{(\sigma_1)_{max}}$: (*a*) $DR-R_p$ interaction; (*b*) t_0-*Strength* interaction; (*c*) R_d-W_r interaction

die design handbook suggests a punch–die clearance range of $(1.75–2.25)t_0$ for stainless steel. Both limits were incorporated separately in the two sets. The corresponding punch force-displacement curves are shown in Fig. 10. The curves in Fig. 10(*a*) indicate that the maximum loads increase with increasing run-off. With a large run-off, more material exists in the radial direction of the die to resist the hoop stress as well as the drawing load. In addition, the fact that the die failed in one experiment

Table 5 Experiments to investigate the effects of punch–die clearance and run-off

Process parameter	Set 1			Set 2		
	Exp 1-1	Exp 1-2	Exp 1-3	Exp 2-1	Exp 2-2	Exp 2-3
Sheet material	304 stainless steel			304 stainless steel		
Sheet thickness t_0	1.22 mm			1.22 mm		
Blank diameter D_0	50.8 mm			50.8 mm		
Punch diameter D_p	28.6 mm			28.6 mm		
Draw ratio DR	1.8			1.8		
Punch–die clearance c	2.75 mm ($2.25t_0$)			2.13 mm ($1.75t_0$)		
Punch corner radius R_p	3 mm	6 mm	6 mm	6 mm		
Die corner radius R_d	6.4 mm			6.4 mm		
Run-off W_r	20 mm	15 mm	10 mm	12 mm	11 mm	10 mm
Punch speed v_p	25.4 mm/min			25.4 mm/min		

(that is, when $W_r = 10$ mm) but not in the others indicates that there exists a critical run-off value below which catastrophic fracture becomes the dominant failure mode.

The curves in Fig. 10(*b*) also exhibit a similar trend of the maximum load increasing as run-off increases, although the trend is not as prominent as in Set 1, as the differences between the run-off values are small. It can be noticed that the maximum load level is higher than that in Set 1 because the lower limit of punch-die clearance ($1.75t_0$) was used. In Set 2, the die failed in all three experiments, and it is important to note how far the punch has traveled at fracture. The punch has traveled past the point of maximum load (or the peak in the curve) in Experiment 2-1, while the die broke before the point of maximum load was reached in Experiments 2-2 and 2-3.

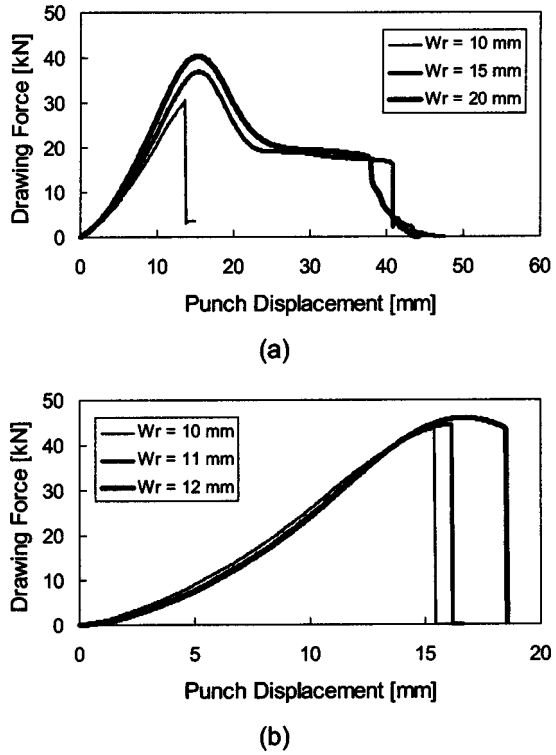

Fig. 10 Effects of punch-die clearance and run-off in cup drawing: (*a*) $c = 2.25t_0$; (*b*) $c = 1.75t_0$

The FEA corresponding to the six experiments were performed, and the resulting greatest maximum principal stresses along with the measured relevant drawing forces are summarized in Table 6. As has been discussed, a typical drawing force curve exhibits a peak and that the die fails (if it fails by rupture) either before or after this peak is reached, depending on whether a critical stress has been reached. The die did not fail in Experiments 1-1 and 1-2; the die failed as the drawing force was increasing in Experiments 1-3, 2-2, and 2-3; the die failed as the drawing force was decreasing past its peak in Experiment 2-1. In Experiment 2-1, although the force curve showed a decreasing trend past the peak, $(\sigma_1)_{\max}$ was constantly increasing until the die fractured at 58.4 MPa.

In both sets of results, $(\sigma_1)_{\max}$ follows an increasing trend as the run-off becomes smaller. (The stress values in the parentheses marked ** must be considered to notice this trend.) However, Set 2 shows that $(\sigma_1)_{\max}$ at fracture decreases with decreasing run-off. The stresses approximate the flexural strength σ_u of 54 MPa (for Ren Shape™ 5166), which suggests that Eq. (1) can be used as a rough criterion to evaluate the susceptibility to die fracture.

Three representative fracture modes are shown in Fig. 11. The modes are distinguished by the number of cracks (and therefore the number of fractured pieces), which include one-crack, two-crack, and three-crack modes. One observation is that the cracks are equidistanced in the circumferential direction along the die wall. In addition, the number of equidistanced cracks increases as the run-off decreases. As the volume of the material in the radial direction is reduced, the resistance to hoop stresses decreases, thus making more material to be prone to develop a crack followed by fast propagation.

Wear. Two experiments were performed until wear occurred on the die corner, and the relationship between the die geometries and the resulting part defect due to wear was analyzed. The experiment conditions conformed to Set 2 in Table 5, with run-off of 10 mm (Case 1) and 8 mm (Case 2), respectively. Wrinkling is a common phenomenon when a blankholder is not used. As the blankholder is not used in this study, the experiments were displacement-controlled such that the punch was stopped imme-

Table 6 FEA results of cup drawing for comparison with experimental data. * Values at fracture. ** The values that would have been obtained if the die did not fracture.

	Set 1			Set 2		
	Exp 1-1	Exp 1-2	Exp 1-3	Exp 2-1	Exp 2-2	Exp 2-3
$(\sigma_1)_{\max}$ (MPa)	39.2	49.4	28.1* (70.0**)	58.4* (63.9**)	49.8* (71.0**)	47.1* (81.1**)
Punch force at $(\sigma_1)_{\max}$ (kN)	30.0	34.3	30.5*	43.6*	44.5*	43.6*
Peak punch force (kN)	40.4	37.0	30.5*	46.0	44.5*	43.6*

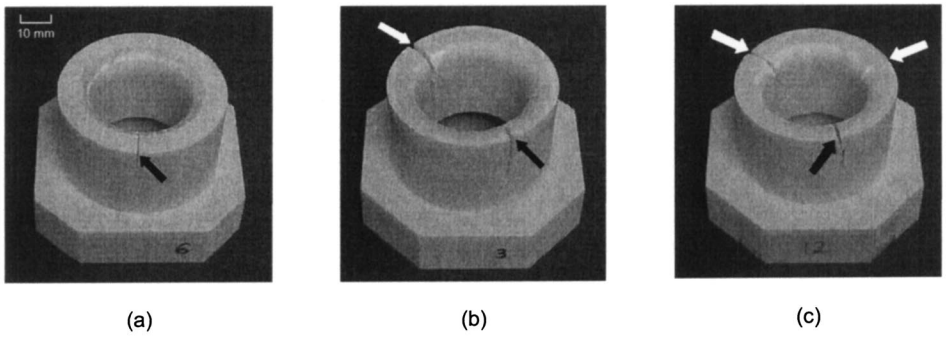

Fig. 11 Representative fracture modes: (*a*) one-crack mode; (*b*) two-crack mode; (*c*) three-crack mode

diately before the wrinkles began to develop. The load and punch displacement were recorded for each drawing operation. The die was determined to have failed by wear when enough material was removed from the die surface to cause wrinkling. The wear volume was not quantified, as it was beyond the scope of this research.

A summary of Cases 1 and 2 is shown in Table 7. The corresponding FEA was performed to obtain stress tensors, from which the maximum normal component of the traction vector $(T_n)_{\max}$ was calculated. In relation to the Archard's expression (Eq. (2)), $(T_n)_{\max}$ can be used to evaluate wear volume qualitatively. A smaller punch displacement was applied in Case 2, which resulted in a smaller maximum drawing force. However, $(T_n)_{\max}$ is slightly greater, which indicates that reducing the run-off increases the normal pressure on the die corner. This does not guarantee that the wear volume will be greater in Case 2, as wear volume also is a function of the sliding distance. As the punch displacement is smaller in Case 2, the sliding distance is smaller as well.

The progression of wear and the corresponding parts for Case 1 are presented in Fig. 12. It can be seen that wear began to take place between the tenth and the 60-th part, indicated by the photos of the die surfaces as well as the wrinkling in the sheet metal parts. The location of wrinkling corresponds to the site where material has been eroded away from the die surface. The degree of wrinkling became more severe as the drawing operation progressed. For Case 2, total of 250 parts were produced, and the onset of wrinkling occurred between the 100-th and the 150-th part.

Table 7 Wear experiment summary

	Case 1	Case 2
Run-off W_r	10 mm	8 mm
Punch displacement (measured)	11.6 mm	10.1 mm
Maximum drawing force (measured)	31.1 kN	27.6 kN
$(T_n)_{\max}$ (from FEA)	137 MPa	140 MPa
Number of parts produced	147	250

Plastic Deformation. Plastic deformation in the die occurred when the sheet metal underwent wrinkling and the wrinkled ''flange'' formed during an intermediate stage of cup drawing subjected the die corner to large compressive normal stresses. A die that failed due to plastic deformation revealed equidistanced depressions along the corner radius caused by the planar anisotropy of the sheet metal, which depends on its rolling direction. The relationship between wrinkling and die stresses, which is associated with plastic deformation in the die, requires three-dimensional analysis and is left for future work.

The mode and the effect of plastic deformation in the punch also are of significant interest. Three punches with corner radii of 3 mm (Punch 1) and 6 mm (Punches 2 and 3), after producing 2, 83, 413 parts, respectively, are presented in Fig. 13. The common deformation mode, with varying degrees, is the bulging at the punch corner due to repetitive compressive loading. The amounts of bulging were 0.35, 0.18, and 0.01 mm in radial direction, respectively. Punches 1 and 2 were used to form the parts past the point of maximum drawing force (which is the peak in the force curve), while Punch 3 was used to form the parts before wrinkling took place (which typically required the force below the maximum load). The amount of bulging indicates that the plastic de-

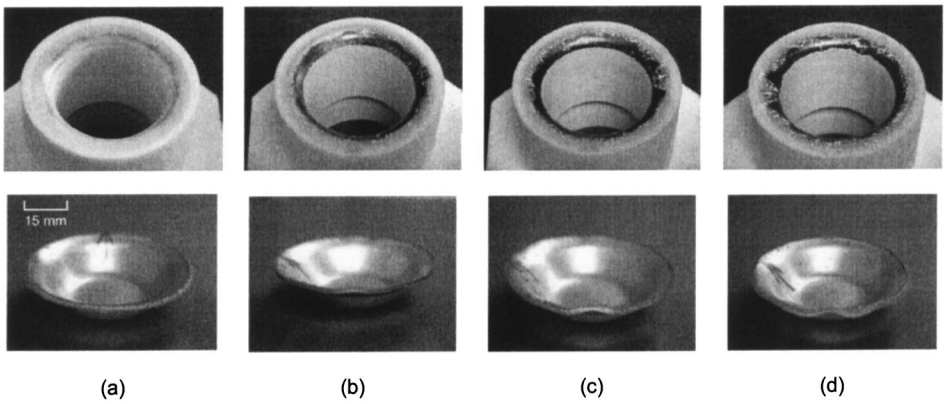

Fig. 12 Progressive formation of die wear after (*a*) 10 parts; (*b*) 60 parts; (*c*) 110 parts; (*d*) 140 parts

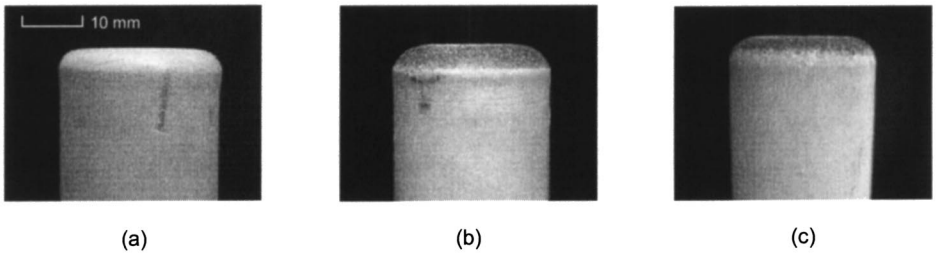

Fig. 13 Plastic deformation in the punch: (*a*) R_p=3 mm (2 parts); (*b*) R_p=6 mm (83 parts); (*c*) R_p=6 mm (413 parts)

formation in a punch depends heavily on punch force and punch corner radius. The larger the punch force and the smaller the punch corner radius, the larger the bulge.

Figure 14 shows the distribution of the greatest normal component of the traction vector (in compression) along the punch corner radius. It can be seen from the figure that when the punch corner radius is reduced by half, the normal traction nearly doubles. This explains why plastic deformation took place much sooner when the punch corner radius was 3 mm, as compared to 6 mm. In practical applications, the deformation of the punch should be closely monitored, as the bulge formation leads to increased punch force and reduced punch–die clearance, which may cause part defect, undesired ''ironing'' in the cup wall, or premature die failure due to increased die stresses.

5.3 General Die Design Guidelines. For cylindrical cup drawing, most of the die design rules established for conventional metal dies are applicable, as they are based on the forming of the workpiece rather than the deformation and failure of the die. However, there are several factors to consider when designing with composite dies, such as from Ren Shape™ 5166. One of the most important issues is determining the optimal run-off. It goes without saying that the larger run-off provides greater resistance to hoop stress and reduces the likelihood of fracture failure. However, from the material handling and economics standpoints, the run-off can be optimized, that is, it can be selected to be large enough to prevent fracture and small enough to minimize cost. The experimental results showed that the die undergoes fracture when the maximum tensile principal stress reaches the vicinity of the flexural strength of the tooling material. Therefore, the FEA with an axisymmetric model should be performed to obtain the hoop stresses, which are equal to the maximum tensile principal stresses, and these stresses should be compared to the flexural strength. However, care must be taken, as this method can be used only as a rough guideline.

It is desirable to apply the largest punch–die clearance allowable, as long as the final drawn part meets the geometric tolerances. A large clearance is beneficial in both fracture and wear prevention, as it reduces hoop and normal stresses on the die surface. Another design parameter to consider is the punch corner radius. Therefore, the part should be designed such that the punch corner radius, which determines the corner radius of the drawn cup, is maximized. The experiments have shown that a small corner radius tends to increase the pressure on the punch surface leading to plastic deformation under compression.

6 Conclusions

This paper developed and verified a method for predicting the failure mode of a cylindrical cup drawing die fabricated from an ATH-filled thermoset polyurethane tooling board (Ren Shape™ 5166). The stress states in the die, which govern the failure, are not intuitive, and thus require computational simulations. The simulations were performed by constructing a FE model and obtaining the stress–strain responses. The possible failure modes in cylindrical cup drawing dies are fracture, wear, and plastic deformation. The damage parameters used were the maximum tensile principal stress for fracture and the maximum normal component of a traction vector on the die surface for wear. Plastic deformation occurs primarily due to the wrinkles in the sheet metal when no blankholder is used. The drawing die fails when the maximum principal stress reaches the flexural strength of the die material. One important observation is that the peak in the drawing force curve does not correspond to the maximum stress, which necessitates the FEA of the process prior to selecting process parameters.

A statistical analysis of the two-level fractional factorial design showed that sheet strength and thickness are the most dominant parameters, followed by draw ratio, punch–die clearance, and run-off. The analysis also revealed that several influential two-factor interactions exist, including the punch corner radius-draw ratio, sheet strength-thickness, and die corner radius-run-off interactions. The experimental study showed that the punch corner radius must be selected carefully to prevent premature plastic deformation failure of the die.

In conclusion, this study provided a method to predict the failure mode of a cylindrical cup drawing die and the die design

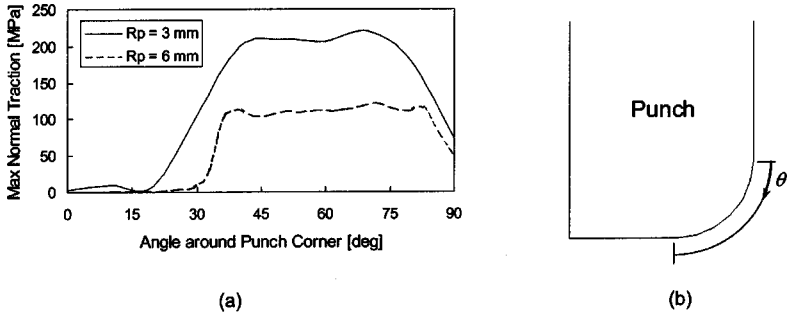

Fig. 14 Effect of punch corner radius on normal traction: (*a*) Normal traction distribution along punch corner; (*b*) angle around punch corner

guidelines that can be employed in the preliminary design stage. The research identified the valid damage parameters for various die failure modes, based on the underlying failure mechanisms. Parametric studies were performed to identify influential parameters and interactions that contribute to die failure. The study laid the groundwork for tool failure and life prediction for general, low-ductility, powder-filled thermoset composite with applications in general sheet metal forming operations.

Acknowledgment

The authors gratefully acknowledge Vantico Inc. for their technical support and supply of their products. The authors also would like to thank Professors David McDowell, Christopher Lynch, Min Zhou, and Richard Neu in the George W. Woodruff School of Mechanical Engineering at Georgia Institute of Technology for technical support and helpful discussions. Cup drawing experiments were made possible by the support of the Mechanical Properties Research Laboratories at the Georgia Institute of Technology.

References

[1] Aronson, R. B., 1998, ''Toolmaking through Rapid Prototyping,'' Manuf. Eng., **11**, pp. 52–56.
[2] Miller, W., 1999, ''Production Dies for Rapid Prototyping of Metal Formed Parts,'' Fabricator **29**(4), pp. 44–47.
[3] Du, Z. H., Chua, C. K., Chua, Y. S., Loh-Lee, K. G., and Lim, S. T., 2002, ''Rapid Sheet Metal Manufacturing. Part 1: Indirect Rapid Tooling,'' Int. J. Adv. Manuf. Technol., **19**, pp. 411–417.
[4] Cheah, C. M., Chua, C. K., Lee, C. W., Lim, S. T., Eu, K. H., and Lin, L. T., 2002, ''Rapid Sheet Metal Manufacturing. Part II: Direct Rapid Tooling,'' Int. J. Adv. Manuf. Technol., **19**, pp. 510–515.
[5] Park, Y., 2003, ''Sheet Metal Forming Using Rapid Prototyped Tooling,'' Ph.D. thesis, Georgia Institute of Technology.
[6] Jensen, M. R., Damborg, F. F., Nielsen, K. B., and Danckert, J., 1998, ''Applying the Finite Element Method for Determination of Tool Wear in Conventional Deep Drawing,'' J. Mater. Process. Technol., **83**, pp. 98–105.
[7] Jensen, M. R., Damborg, F. F., Nielsen, K. B., and Danckert, J., 1998, ''Optimization of the Draw Die Design in Conventional Deep Drawing in Order to Minimize Tool Wear,'' J. Mater. Process. Technol., **83**, pp. 106–114.
[8] Christiansen, S., and de Chiffre, L., 1997, ''Topographic Characterization of Progressive Wear on Deep Drawing Dies,'' STLE Tribol. Trans., **40**(2), pp. 346–352.
[9] Siegert, K., and Haller, B., 1998, ''Prototype Draw Dies for Sheet Metal Parts,'' Developments in Sheet Metal Stamping, Warrendale, PA, SAE SP-1322, pp. 41–51.
[10] Sachs, G., 1966, *Principles and Methods of Sheet Metal Fabricating*, 2nd ed., Reinhold Publishing Corporation, New York.
[11] Kalpakjian, S., 1997, *Manufacturing Processes for Engineering Materials*, 3rd ed., Addison-Wesley, Menlo Park, CA.
[12] American Society of Tool and Manufacturing Engineers, 1965, *Die Design Handbook*, 2nd ed., McGraw-Hill, New York, NY.
[13] *Metals Handbook*, Desktop Edition, edited by H. E. Boyer and T. L. Gall, American Society for Metals, 1985.
[14] Kocanda, A. Z., and Raddad, B., 1992, ''Elasto-Plastic Deformation Behavior and Fracture of Ring-Shaped Dies,'' J. Mater. Process. Technol., **34**, pp. 181–186.
[15] *Fatigue and Tribological Properties of Plastics and Elastomers*, Plastics Design Library, Norwick, NY, 1995.
[16] Tadmor, Z., and Gogos, C. G., 1979, *Principles of Polymer Processing*, John Wiley and Sons, New York, NY.
[17] Neter, J., Kutner, M. H., Nachtsheim, C. J., and Wasserman, W., 1996, *Applied Linear Statistical Models*, 4th ed., McGraw-Hill, New York, NY.